ADVANCED FUNCTIONAL MATERIALS
www.afm-journal.de

Conjugated Polyelectrolyte Hybridized ZnO Nanoparticles as a Cathode Interfacial Layer for Efficient Polymer Light-Emitting Diodes

*Kyungmok Kim, Minwon Suh, Jihae Choi, Dongchan Lee, Youngsun Kim, Sang Hun Cheong, Donghyuk Kim, and Duk Young Jeon**

Alkoxy side-chain tethered polyfluorene conjugated polyelectrolyte (CPE), poly[(9,9-bis((8-(3-methyl-1-imidazolium)octyl)-2,7-fluorene)-alt-(9,9-bis(2-(2-methoxyethoxy)ethyl)-fluorene)] dibromide ($F8imFO_4$), is utilized to obtain CPE-hybridized ZnO nanoparticles (NPs) (CPE:ZnO hybrid NPs). The surface defects of ZnO NPs are passivated through coordination interactions with the oxygen atoms of alkoxy side-chains and the bromide anions of ionic pendent groups from $F8imFO_4$ to the oxygen vacancies of ZnO NPs, and thereby the fluorescence quenching at the interface of yellow-emitting poly(*p*-phenylene vinylene)/CPE:ZnO hybrid NPs is significantly reduced at the CPE concentration of 4.5 wt%. Yellow-emitting polymer light-emitting diodes (PLEDs) with CPE(4.5 wt%):ZnO hybrid NPs as a cathode interfacial layer show the highest device efficiencies of 11.7 cd A^{-1} at 5.2 V and 8.6 lm W^{-1} at 3.8 V compared to the ZnO NP only (4.8 cd A^{-1} at 7 V and 2.2 lm W^{-1} at 6.6 V) or CPE only (7.3 cd A^{-1} at 5.2 V and 4.9 lm W^{-1} at 4.2 V) devices. The results suggest here that the CPE:ZnO hybrid NPs has a great potential to improve the device performance of organic electronics.

1. Introduction

Polymer light-emitting diodes (PLEDs) have attracted a great attention as a possibility for next-generation large-area display and lighting devices due to solution processability and low energy-consumption property.[1,2] Still improving the device performance is one of the main concerns for successful commercialization of PLEDs. In PLEDs, generally injected holes tend to be accumulated at the interface between emissive layer (EML) and cathode electrode rather than injected electrons building up at the anode interface.[3–8] The use of cathode interfacial layer (CIL) is essential in order to not only provide better electron injection/transport abilities but also block the excess holes and minimize the loss in injected charge carriers not being able to form excitons, thus maximize radiative recombination rate. A strategy to develop solution-processable charge injection material for CIL is highly demanded for realizing high-efficiency PLEDs.[3–9]

In this context, many approaches have been reported in the literature up to date. Zinc oxide (ZnO) has been extensively investigated as a CIL in organic optoelectronics to enhance device performance by taking advantage of deep valence band (VB) of ≈7.8 eV with a large band gap of ≈3.4 eV and high intrinsic electron mobility of ≈200 $cm^2\ V^{-1}\ S^{-1}$.[7,10,11] ZnO nanoparticles (NPs) can be prepared through facile synthetic methods in ambient conditions and are stable in colloidal state when dispersed in common polar organic solvents.[12–14] This allows ZnO NPs to be deposited on top of typical organic semiconducting layers without damaging the underlying layer. However, ZnO NPs have a significant number of surface defects likely oxygen vacancy due to a large surface-to-volume ratio that could be potential electron trap sites.[15–18] It is also known that ZnO NPs can induce exciton quenching of light-emitting polymer (LEP) in two different paths; (i) energy transfer process from LEP to the defect level of ZnO NPs and (ii) exciton dissociation via excited-state electron transfer process from LEPs to ZnO NPs.[9,19–22] Furthermore, a large energy barrier between the lowest unoccupied molecular orbital (LUMO) of light-emitting polymers and the conduction band (CB) of ZnO makes electron injection difficult and less favorable.[5–9,23] It is reported that an additional thin interfacial layer, such as cesium carbonate (Cs_2CO_3), self-assembled monolayers (SAMs), and conjugated polyelectrolytes (CPEs), on ZnO layer helps to lower the energy barrier by introducing interfacial dipole effect.[5–8,23,24]

K. Kim, Dr. M. Suh,[+] J. Choi, D. Lee, S. H. Cheong, Dr. D. Kim,[++] Prof. D. Y. Jeon
Department of Materials Science and Engineering
Korea Advanced Institute of Science and Technology (KAIST)
291 Daehak-ro, Yuseong-gu
Daejeon 305-701, South Korea
E-mail: dyjeon@kaist.ac.kr

Y. Kim
Center for Theragnosis
Korea Institute of Science and Technology (KIST)
39-1 Hawolgok-dong, Seongbuk-gu, Seoul 136-791, South Korea

[+]Present address: Department of Physics and Centre for Plastic Electronics, Imperial College London, Prince Consort Road, London SW7 2AZ, UK

[++]Present address: Battery R&D, LG Chem. Ltd., 188, Munji-ro, Yuseong-gu, Daejeon 305-738, South Korea

DOI: 10.1002/adfm.201502360

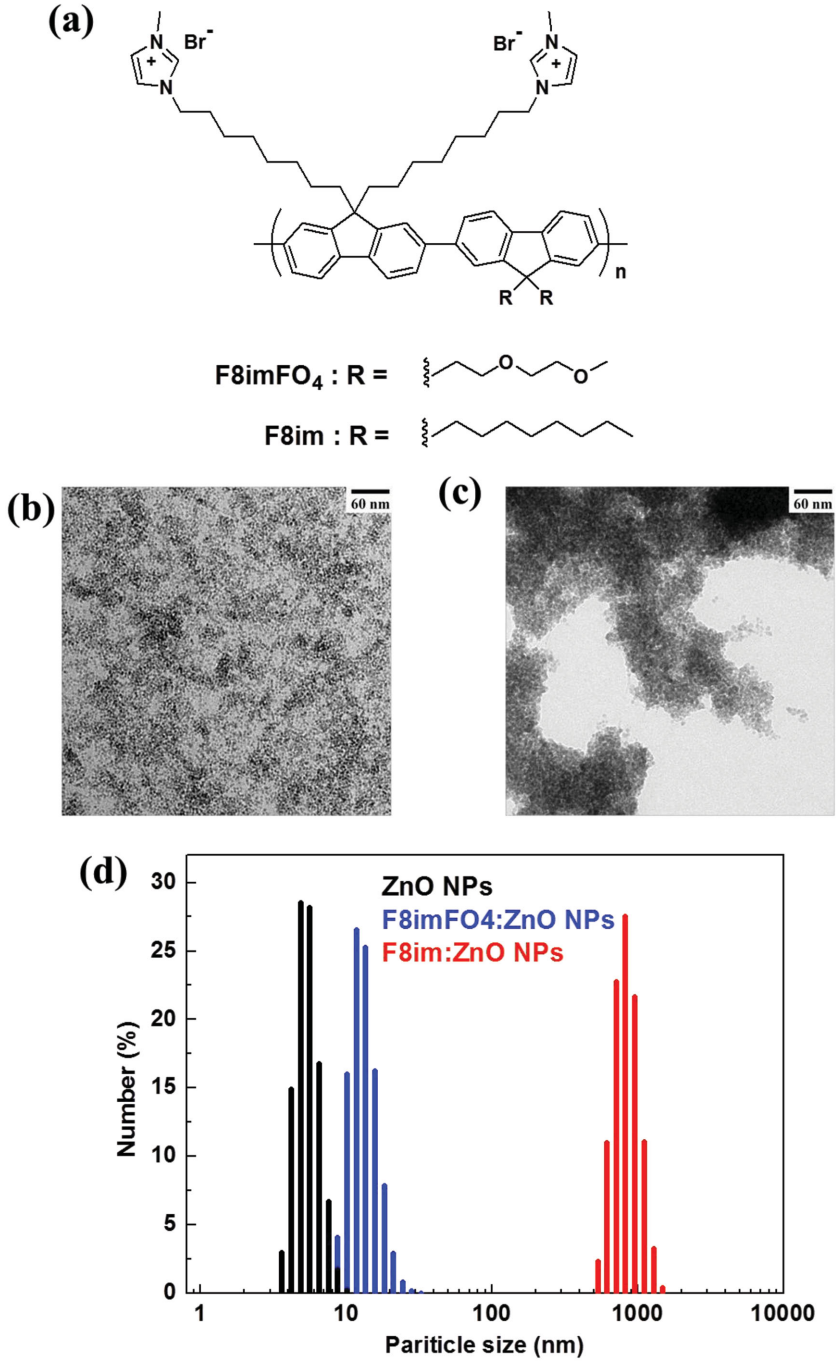

Figure 1. a) Chemcial structure of $F8imFO_4$ and F8im CPEs. TEM images of CPE:ZnO hybrid NPs with different CPEs; b) $F8imFO_4$:ZnO NPs and c) F8im:ZnO NPs. The scale bar is 60 nm. d) Particle size distribution of ZnO NPs and CPE:ZnO hybrid NPs in 2-methoxyethanol. The concentration of CPE is fixed at 9 wt% in both cases.

Herein, we present CPE-hybridized ZnO NPs (CPE:ZnO hybrid NPs), so-called organic/inorganic hybrid material, as a solution-processable CIL for high-efficiency PLEDs. Alkoxy side-chain tethered polyfluorene CPE, poly[(9,9-bis((8-(3-methyl-1-imidazolium)octyl)-2,7-fluorene)-alt-(9,9-bis(2-(2-methoxyethoxy)ethyl)-fluorene)] dibromide ($F8imFO_4$, **Figure 1**a), was synthesized in order to offer not only good miscibility with ZnO NPs for preventing phase separation but also make use of the charged nature of CPE for better electron injection at EML/electrode interface. X-ray photoelectron spectroscopy (XPS) analysis results reveal that the surface defects of ZnO NPs are passivated by forming two different kinds of coordination bond with functional groups, alkoxy side-chains and bromide anions, from $F8imFO_4$. We find that a specific CPE concentration (4.5 wt% to the weight of ZnO NPs) shows the most efficient passivation effect of ZnO NPs and reduces photoluminescence (PL) quenching of yellow-emitting PPV layer (commercial name "Super Yellow," SY). Consequently, the device efficiencies of SY-based PLEDs are greatly increased with the CPE:ZnO hybrid NPs (11.7 cd A^{-1} at 5.2 V and 8.6 lm W^{-1} at 3.8 V) compared to the PLEDs with ZnO NPs only (4.8 cd A^{-1} at 7 V and 2.2 lm W^{-1} at 6.6 V) or $F8imFO_4$ CPE only (7.3 cd A^{-1} at 5.2 V and 4.9 lm W^{-1} at 4.2 V).

2. Results and Discussion

$F8imFO_4$ CPE was synthesized through Suzuki cross-coupling polymerization, followed by substitution reaction using *n*-methylimidazole to functionalize imidazolium bromide ionic pendent group on alkoxy side-chain tethered polyfluorene.[25,26] The resulting polymer, $F8imFO_4$, is soluble in typical polar organic solvents such as 2-methoxyethanol. F8im CPE was similarly prepared. For the preparation of colloidal ZnO solutions, ZnO NPs were synthesized using zinc acetate dihydrate and lithium hydroxide monohydrate as precursors in ethanol.[14] The X-ray diffraction (XRD) result identifies that the crystal structure of the ZnO NPs is corresponding to wurtzite structure of ZnO (Figure S1, Supporting Information). $F8imFO_4$ at desired concentration to the weight of ZnO NPs was added to the colloidal solution in 2-methoxyethanol to obtain the CPE:ZnO hybrid NPs. (See the details of the synthetic procedures in the Supporting Information.)

Figure 1b,c shows the transmission electron microscopy (TEM) images of CPE:ZnO hybrid NPs using two different CPEs; $F8imFO_4$ and F8im, respectively. It is observed that ZnO NPs are uniformly dispersed in the case of the hybrid NPs with $F8imFO_4$, whereas ZnO NPs blended with F8im form agglomerated clusters. Note that the concentration of CPEs was fixed at 9 wt% for both hybrid NPs. The particle size distribution results in Figure 1d, analyzed by dynamic

light scattering (DLS) technique, clearly indicate that CPE:ZnO hybrid NPs with $F8imFO_4$ show a better dispersion of the particles (13.4 nm) than that of CPE:ZnO hybrid NPs with F8im (820 nm). The particle size distribution of ZnO NPs on its own (5.5 nm) matches well with the diameter confirmed in the TEM image (Figure S2, Supporting Information). Although the size of ZnO NPs for the CPE($F8imFO_4$):ZnO hybrid NPs seem to be the same in the TEM image, the particle size distribution is increased to 13.4 nm, implying that the hybrid NPs possibly form nanoclusters with 3–5 of particles combined together. In contrast, in the case of CPE(F8im):ZnO hybrid NPs, both the TEM image and the particle size distribution show the submicrometer-sized agglomerates. This result potentially suggests that the incorporation of alkoxy side-chains from $F8imFO_4$ CPE plays a key role in interacting with ZnO NPs and therefore preventing ZnO NPs being aggregated each other.

To give insight into the chemical interaction between ZnO NPs and $F8imFO_4$ CPE, we utilzed XPS technique for thin films of the ZnO NPs, CPE, and CPE(9 wt%):ZnO hybrid NPs deposited on top of indium-tin-oxide (ITO) substrates (**Figure 2**).

The O 1s core level spectra of the ZnO NPs, CPE, and CPE:ZnO hybrid NPs are shown in Figure 2a–c. The ZnO NPs

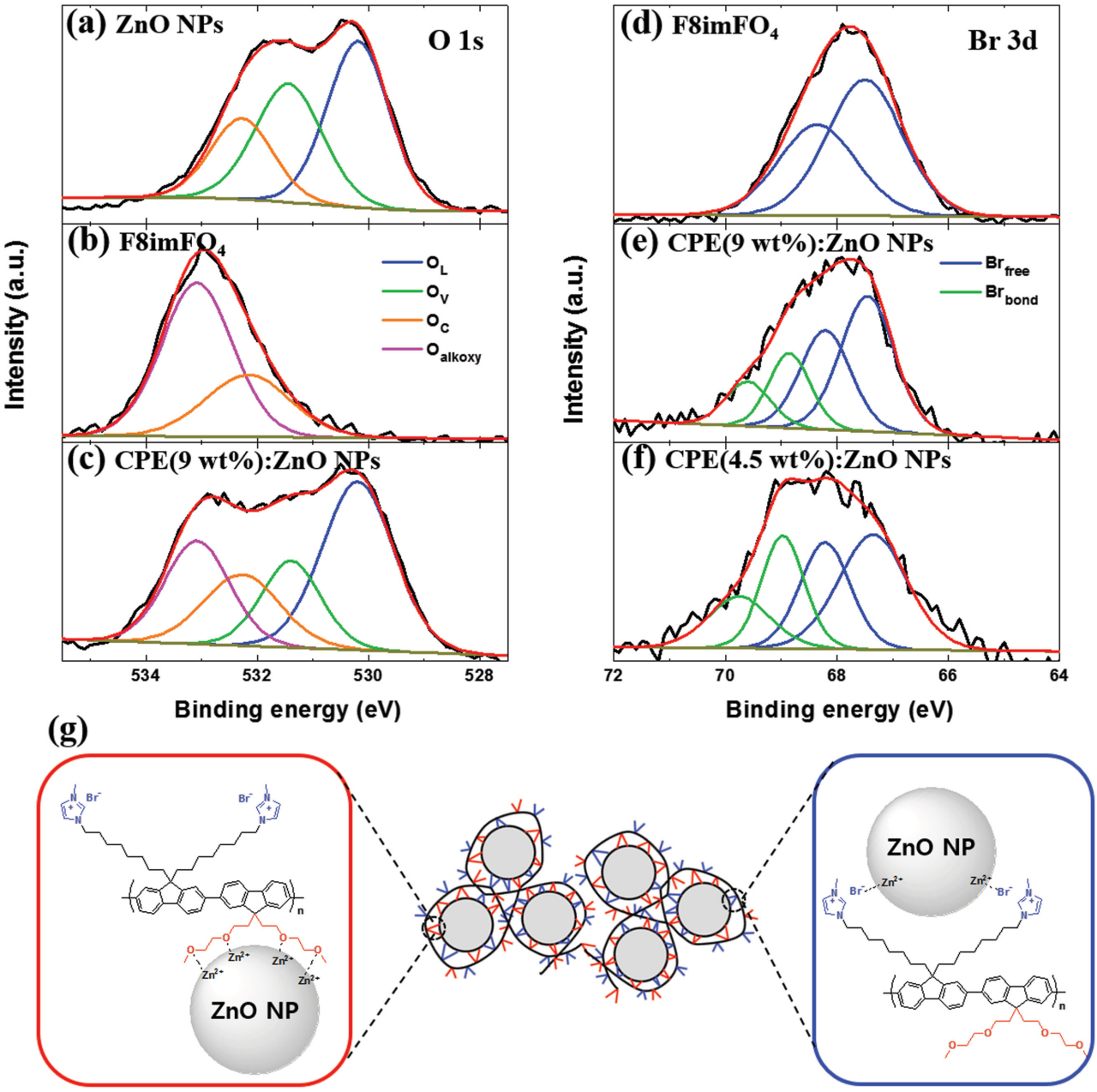

Figure 2. XPS core level spectra of O 1s; a) ZnO NPs, b) $F8imFO_4$, and c) CPE(9 wt%):ZnO hybrid NPs. XPS core level spectra of Br 3d; d) $F8imFO_4$, e) CPE(9 wt%):ZnO NPs, and f) CPE(4.5 wt%):ZnO NPs. Black and red curves are experimental data and fitted plots, respectively. g) A schematic illustration of CPE:ZnO hybrid NPs.

Table 1. XPS binding energies of O 1s and Br 3d and their relative percentages.

	O 1s binding energy [eV] (relative percentage [%])				Oxygen vacancy ratio	Br 3d binding energy [eV] (relative percentage [%])				Bromide bonding ratio
	Lattice oxygen (O_L)	Vacant oxygen (O_V)	Chemisorbed oxygen (O_C)	C–O (O_{alkoxy})	O_V/O_L	Free Br (Br_{free})		Zn–Br (Br_{bond})		Br_{bond}/Br_{free}
						$3d_{5/2}$	$3d_{3/2}$	$3d_{5/2}$	$3d_{3/2}$	
ZnO NPs	530.2 (44.0)	531.4 (34.4)	532.3 (21.6)	–	0.782	–	–	–	–	–
$F8imFO_4$	–	–	532.2 (32.4)	533.1 (67.6)	–	67.5 (59.2)	68.3 (40.8)	–	–	0
CPE(9 wt%):ZnO NPs	530.2 (41.0)	531.4 (17.6)	532.3 (18.4)	533.1 (23.0)	0.429	67.5 (41.8)	68.2 (28.9)	68.8 (17.6)	69.6 (11.7)	0.414
CPE(4.5 wt%):ZnO NPs	–	–	–	–	–	67.4 (37.2)	68.2 (24.9)	69.0 (22.7)	69.8 (15.2)	0.610

possess three distinctive states appearing at 530.2, 531.4, and 532.3 eV, which correspond to oxygen anion (O^{2-}) species in ZnO lattice (O_L, blue curve), oxygen vacancy (O_V, green curve), and chemisorbed moieties on the surface (O_C, organge curve), respectively.[4–6] The chemisorbed sites are likely to be hydroxyl and/or carbonate groups being attached to the ZnO NP surface.[15,16,27] $F8imFO_4$ also contains a considerable amount of the chemisorbed oxygen component appearing at the same binding energy region of 532.3 eV, which is possibly due to hydrophilic nature of the CPE.[28] The stronger peak centered at 533.1 eV in the O 1s core level spectrum of $F8imFO_4$ is assigned to carbon–oxygen bond (O_{alkoxy}, magenta curve) in the alkoxy side-chain of the CPE structure.[29] The O 1s spectrum of the CPE:ZnO hybrid NPs consists of the four features from both ZnO NPs and CPE with no additional peaks, implying that the blending of these two materials does not lead to the formation of new chemical speices.

The oxygen vacancy ratio (O_V/O_L), defined as a ratio of oxygen vacancy and lattice oxygen, is introduced in **Table 1**. The chemisorbed component is excluded as this is likely influenced by surroundings such as residual solvent molecules and/or moisture in air.[15,16,27] It is estimated that the oxygen vacancy ratio for ZnO NPs is 0.782 whereas the value is 0.429 for CPE:ZnO hybrid NPs. Note that the difference in the relative percentage of oxygen lattice in ZnO NPs between with and without $F8imFO_4$ CPE is only 3% (41.0 vs 44.0%). Based on the fact that the oxygen lattice is mostly concentrated in the inner crystalline core of ZnO NPs and therefore is less affected by the addition of $F8imFO_4$, the oxygen vacancy is scattered at the outer surface and would have more chance to interact with the oxygen of the alkoxy side-chain.[15,16] As a result, the addition of $F8imFO_4$ seems to help reducing oxygen vacancies in ZnO NPs.

Figure 2d–f shows the Br 3d core level spectra of the CPE and CPE(9 wt%):ZnO hybrid NPs. The CPE only film has two coupled peaks centered at 67.5 (Br $3d_{5/2}$) and 68.3 eV (Br $3d_{3/2}$), corresponding to non-coordinated bromide state (Br_{free}, blue curve) from bromide counter anions of the imidazolium cations.[30] There is an evolution of a higher binding energy shoulder at 69 eV (green curve) for the CPE:ZnO hybrid NP cases. The 69 eV peak can be considered as a lithium–bromine bond character because there might be a trace amount of the lithium residues left in the ZnO NP solution from the synthesis process.[31] However, no lithium signal observed in the XPS survey and thus no impurities involved (Figure S3, Supporting Information). It is likely to be the case that the bromide anions are coordinated to the zinc cations on the surface of ZnO NPs. The weaker binding energy (69 eV) observed for zinc-bromine bond in our study compared with the value reported in the literature (70 eV) on zinc bromide ($ZnBr_2$) compounds would be due to a large difference in the ionic radius between bromide anion (196 pm) and oxygen anion (138 pm).[32–34]

Bromide bonding ratio (Br_{bond}/Br_{free}) is defined as a ratio of bromide in coordination with the zinc of ZnO NPs to bromide in non-coordinated state (Table 1). It is estimated that the bromide bonding ratio is 0.610 for 4.5 wt% CPE added hybrid NPs while it is 0.414 for the 9 wt% CPE case. The decrease in the ratio for higher CPE concentration in the blend is possibly due to an excessive amount of the bromide anions, leaving the non-coordinated bromide state.

Our XPS study suggests that not only the alkoxy side-chain but also the bromide counter anion of $F8imFO_4$ have ability to form coordination bonding with the zinc cations on the surface of ZnO NPs and therefore reduce the oxygen vacancies. Contact angles of a water drop on the ZnO NP and CPE only layers on top of SY-PPV thin film are 56° and 60°, respectively. However, contact angles are ranging around 60° for the CPE:ZnO hybrid NPs regardless of the CPE concentrations (Figure S4, Supporting Information). This provides the idea that ZnO NPs are being covered with $F8imFO_4$ CPE by taking account of the chemical interactions examined in the XPS analysis (Figure 2g).

In order to explore the impact of the CPE:ZnO hybrid NPs on device performance of organic electronics, standard PLEDs with SY-PPV EML were investigated (**Figure 3**a). Figure 3b shows the current density–voltage–luminance (*J–V–L*) characteristics of SY-PPV PLEDs with CPE:ZnO hybrid NPs as a CIL at different CPE concentrations; 4.5, 9, 18 wt%. Devices incoporating ZnO NP and $F8imFO_4$ CPE layers were also fabricated as a reference, respectively. **Table 2** summarizes the device performance of these five PLEDs.

There is a noticeable change in the current density below turn-on voltage which is defined as voltage required achieving 1 cd m^{-2}. The level of leakage current is the highest for the ZnO NP only device and tends to decrease systematically with an increasing CPE concentration in the CPE:ZnO hybrid NPs. Atomic force microscopy (AFM) topography images of ZnO NP only and CPE(9 wt%):ZnO hybrid NP layers on top of SY-PPV thin film demonstrate a uniform morphology with similar surface roughness values (root mean square of 1.71 and

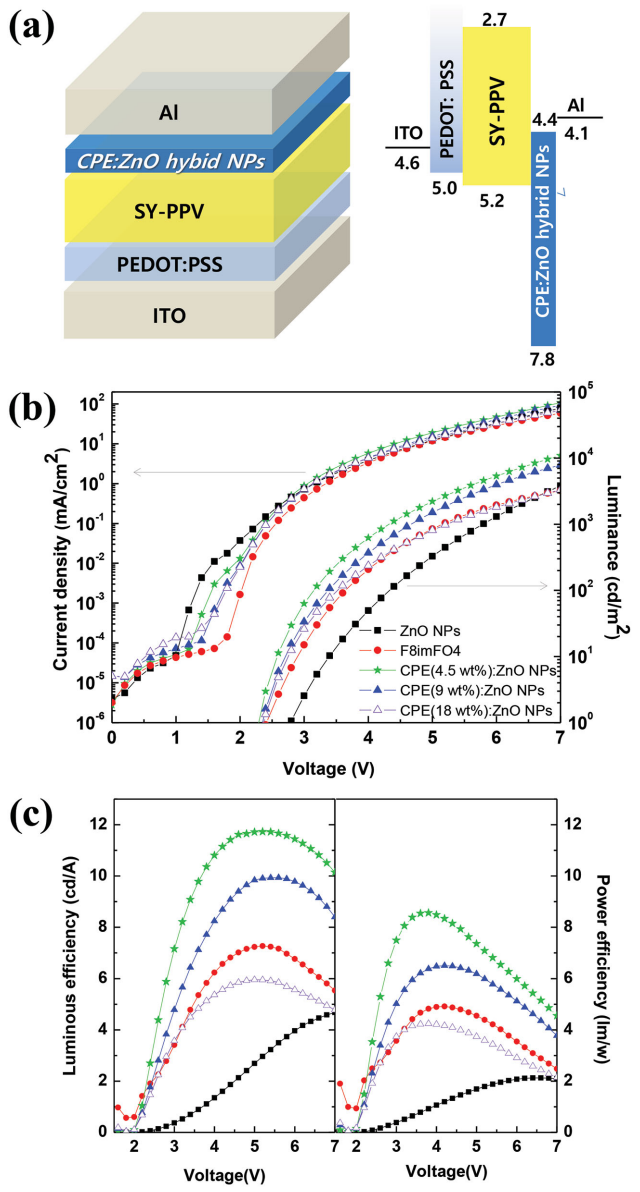

Figure 3. a) Device configuration of SY PLED and its energy level diagram (in the unit of eV). The energy levels of CPE:ZnO hybrid NPs refer to the data obtained on UPS analysis in Figure S7 of the Supporting Information. b) *J–V–L* characteristics of SY PLEDs with different cathode interfacial layers. c) Luminous (cd A^{-1}) and power (lm W^{-1}) efficiencies as a function of applied voltage of the SY PLEDs.

1.65 nm, respectively) (Figure S5, Supporting Information). This suggests that interfacial contact at the CIL/cathode electrode is identical and thus has a negligible effect on the leakage current. The turn-on voltage turned out to be around 2.4 V for all CPE-incorporated devices including the CPE only case, while it is 2.8 V for the ZnO NP only device. Considering the current density of the ZnO NP only device (0.15 mA cm^{-2}) is higher than that of the CPE(4.5 wt%):ZnO hybrid NP device (0.11 mA cm^{-2}) at 2.4 V. Such a high leakage current could be the case where the injected electrons are trapped at the oxygen defects of ZnO NPs and/or transferring along the lateral direction within ZnO NPs.[35,36] However, the CPE:ZnO hybrid NP devices show higher current density (18.80, 15.29, and 13.59 mA cm^{-2} for the CPE concentrations of 4.5, 9, and 18 wt%, respectively) than the ZnO NP only device (12.18 mA cm^{-2}) at 5 V. We observed that change in the luminance is even more dramatic at the same voltage of 5 V; 2202, 1504, and 809 cd m^{-2} for the CPE concentrations of 4.5, 9, and 18 wt%, respectively, and 328 cd m^{-2} for the ZnO NP only.

The electron-only devices (EODs) also demonstrate that the CPE:ZnO hybrid NPs regardless of the CPE concentration show higher current density than the ZnO NP only, implying that the addition of small amount of CPE provides better electron injection capability of ZnO NPs at SY-PPV/Al interface (Figure S6, Supporting Information). Kelvin prove microscopy (KPM) analysis revealed that the workfunction of ZnO NP layer is decreased from 5.09 to 4.90 eV by an addition of 9 wt% of $F8imFO_4$ CPE (Table S1, Supporting Information), indicating that the CPE can induce vacuum level shift of ZnO.[9,37] Therefore, the increase in the current density for the CPE:ZnO hybrid NP devices compared to the ZnO NP only device is considered as a consequence of the reduction of the electron injection barrier at the cathode interface of the PLEDs. This is mainly due to interfacial dipolar polarization induced by the oxygen–ZnO and bromide–ZnO coordination bonding as proved in XPS survey.[23,37,38]

Figure 3c displays the luminous and power efficiencies as a function of the applied bias of the SY-PPV PLEDs. The highest device efficiency is obtained with the CPE(4.5 wt%):ZnO hybrid NPs; 11.7 cd A^{-1} at 5.2 V and 8.6 lm W^{-1} at 3.8 V. The device efficiencies decrease as the CPE concentration increases in the CPE:ZnO hybrid NPs. The ZnO NP only device shows the lowest efficiencies of 4.8 cd A^{-1} at 7 V and 2.2 lm W^{-1} at 6.6 V.

Figure 4 shows the transient PL decay curves of SY-PPV thin films with different CILs measured using a time-correlated single photon counting (TCSPC) technique. The transient PL

Table 2. The device performance of SY-PPV PLEDs with various cathode interfacial layers.

Cathode interfacial layer	Turn-on voltage [V @ 1 cd m^{-2}]	Luminous efficiency		Power efficiency	
		[cd A^{-1} @ bias]	[L, cd m^{-2}]	[lm W^{-1} @ bias]	[L, cd m^{-2}]
ZnO NPs	2.8	4.8 @ 7	3,804	2.2 @ 6.6	2533
$F8imFO_4$	2.4	7.3 @ 5.2	1,044	4.9 @ 4.2	294
CPE(4.5 wt%):ZnO NPs	2.4	11.7 @ 5.2	2,682	8.6 @ 3.8	441
CPE(9 wt%):ZnO NPs	2.4	9.9 @ 5.4	2,294	6.5 @ 4.2	513
CPE(18 wt%):ZnO NPs	2.4	6.0 @ 5.0	809	4.2 @ 3.8	170

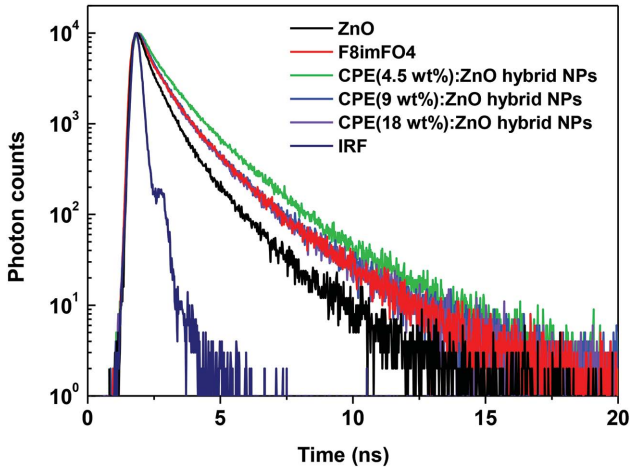

Figure 4. Transient PL decay curves of SY-PPV thin films (≈10 nm) contacted with different cathode interfacial layers.

decays were recorded at the maximum PL peak of SY-PPV (550 nm) excited by 470 nm in vacuum. The PL decay time of SY-PPV with ZnO NP layer is only 0.70 ns, whereas that of SY-PPV with the CPE:ZnO hybrid NP layers at difference CPE concentrations of 4.5, 9, and 18 wt% are 1.20, 1.00, and 0.99 ns, respectively. (Table S2, Supporting Information). Note that charge separation and/or energy transfer process at the interface of LEP/ZnO is responsible for the PL quenching due to the deep-lying CB and surface defects of ZnO NPs.[9,19–22] The CPE:ZnO hybrid NP at lower CPE concentration of 2.25 wt% showed a rather fast PL decay curve with the PL decay time of 0.84 ns (Figure S9, Supporting Information) and the device efficiencies for the corresponding PLED turned out to be only 9.1 cd A^{-1} at 6.8 V and 5.2 lm W^{-1} at 4.4 V (Figure S10, Supporting Information). The PL decay time was significantly enhanced, more specifically, in the case of CPE(4.5 wt%):ZnO hybrid NPs. These results indicate that an optimal amount of CPE is necessary for CPE:ZnO hybrid NPs to effectively passivate ZnO NPs, thereby improving chances of exciton recombination in PLEDs.

3. Conclusion

We have prepared CPE-hybridized ZnO NPs by blending alkoxy side-chain tethered F8imFO_4 CPE into ZnO NP colloidal solution. The incorporation of alkoxy side-chains to CPE backbone is beneficial for CPE:ZnO hybrid NP system in that it not only enables coordination interactions offering good miscibility between the two organic/inorganic heteromaterials but also reduces the surface defects of ZnO NPs. The CPE:ZnO hybrid NPs are uniformly dispersed in common polar organic solvents and readily deposited onto typical organic semiconductor thin films using solution process. Our results successfully demonstrate that the CPE:ZnO hybrid NPs can be used as an efficient CIL in yellow-emitting SY PLEDs. We found that the device efficiencies vary with the amount of F8imFO_4 CPE added in the CPE:ZnO hybrid NPs, which is considered mainly due to the alteration in the defect nature of ZnO NPs with different level of the coordination interactions. Finally, the PLED with CPE:ZnO hybrid NPs at the optimum CPE concentration of 4.5wt% (11.7 cd A^{-1} at 5.2 V and 8.6 lm W^{-1} at 3.8 V) outperforms the devices with ZnO NPs only (4.8 cd A^{-1} at 7 V and 2.2 lm W^{-1} at 6.6 V) or CPE only (7.3 cd A^{-1} at 5.2 V and 4.9 lm W^{-1} at 4.2 V). Our results highlight the fact that a specific amount of CPE is required for CPE:ZnO hybrid NPs in order to effectively passivate ZnO NPs and offer better electron injection for high performance organic electronics. The detailed study of the electronic structure of the CPE:ZnO hybrid NPs is in progress to aid the understanding of the device properties investigated here.

4. Experimental Section

Material Characterizations: TEM images were recorded with a JEOL JEM 3010 at 300 kV. DLS was used on a Malvern Instruments ZEN 3600 Nano-ZS. XPS spectra were achieved using a Sigma Probe (Thermo VG Scientific) with a monochromatic X-ray source of Al Kα 1486 eV at a base pressure of 1×10^{-10} Torr. The XPS spectra were calibrated by carbon–carbon bond as an internal standard of 284.8 eV and deconvoluted by Gaussian–Lorentzian fitting via Advantage software. AFM topographic images were recorded on a XE-70, Park Systems. TCSPC technique was conducted on a FL920, Edinburgh Instruments at a base pressure of 1×10^{-4} Torr.

PLED Device Fabrication and Characterizations: ITO-patterned glass substrates were sonicated in three different solvents (methanol, acetone, and isopropyl alcohol) for 30 min and dried in oven at 120 °C for 30 min, followed by oxygen plasma treatment. A 30 nm thick poly (ehtylenedioxythiophene):poly(styrenesulfonate) (PEDOT:PSS, Clevios P VP AI4083) layer was spin-coated and then annealed at 150 °C for 30 min. A 80 nm thick SY-PPV (Merck, PDY 132) emissive layer was spin-coated from 6 mg mL^{-1} of toluene solution. Subsequently, CILs were spin-coated using either ZnO NP, F8imFO_4 CPE or CPE:ZnO hybrid NP solutions in 2-methoxyethanol to obtain 10 nm thick film on top of the SY-PPV layer. All spin-coating and thermal annealing processes were performed in a nitrogen-filled glovebox. Finally, 120 nm of Al cathode layer was deposited via thermal evaporation method at a base pressure of 1×10^{-7} Torr to complete the device fabrication. The *J–V–L* and efficiencies of PLED devices were measured on a Keithley 2635A source meter unit integrated with a Minolta CS2000 spectrophotometer.

Supporting Information

Supporting Information is available from the Wiley Online Library or from the author.

Acknowledgements

K.K. and M.S. contributed equally to this work. This research was supported and funded by (i) LG Display Co., Ltd., (ii) Basic Science Research Program through the National Research Foundation of Korea (NRF) funded by the Ministry of Education (NRF-2012R1A1A2043856), and (iii) the International Research & Development Program of the National Research Foundation of Korea (NRF) funded by the Ministry of Science, ICT and Future Planning (MSIP) of Korea (NRF-2013K1A3A1A16041887).

Received: June 10, 2015
Revised: September 25, 2015
Published online: November 10, 2015

[1] J. H. Burroughes, D. D. C. Bradley, A. R. Brown, R. N. Marks, K. Mackay, R. H. Friend, P. L. Burns, A. B. Holme, *Nature* **1990**, *347*, 539.
[2] G. Gustafsson, Y. Cao, G. M. Treacy, F. Klavetter, N. Colaneri, A. J. Heeger, *Nature* **1992**, *357*, 477.
[3] T. M. Brown, R. H. Friend, I. S. Millard, D. J. Lacey, J. H. Burroughes, F. Cacialli, *Appl. Phys. Lett.* **2000**, *77*, 3096.
[4] T. M. Brown, R. H. Friend, I. S. Millard, D. J. Lacey, J. H. Burroughes, F. Cacialli, *Appl. Phys. Lett.* **2001**, *79*, 174.
[5] J. Huang, G. Li, E. Wu, Q. Xu, Y. Yang, *Adv. Mater.* **2006**, *18*, 114.
[6] C. V. Hoven, R. Yang, A. Garcia, V. Crockett, A. J. Heeger, G. C. Bazan, T.-Q. Nguyen, *Proc. Natl. Acad. Sci. USA* **2008**, *105*, 12730.
[7] H. J. Bolink, E. Coronado, J. Orozco, M. Sessolo, *Adv. Mater.* **2009**, *21*, 79.
[8] T.-W. Lee, J. Hwang, S.-Y. Min, *ChemSusChem* **2010**, *3*, 1021.
[9] Y.-H. Kim, T.-H. Han, H. Cho, S.-Y. Min, C.-L. Lee, T.-W. Lee, *Adv. Funct. Mater.* **2014**, *24*, 3808.
[10] D. C. Look, D. C. Reynolds, J. R. Sizelove, R. L. Jones, C. W. Litton, G. Cantwell, W. C. Harsch, *Solid State Commun.* **1988**, *105*, 399.
[11] P. Tiwana, P. Docampo, M. B. Johnston, H. J. Snaith, L. M. Herz, *ACS Nano* **2011**, *5*, 5158.
[12] L. Spanhel, M. A. Anderson, *J. Am. Chem. Soc.* **1991**, *113*, 2826.
[13] E. A. Meulenkamp, *J. Phys. Chem. B* **1998**, *102*, 5566.
[14] H.-M. Xiong, R.-Z. Ma, S.-F. Wang, Y.-Y. Xia, *J. Mater. Chem.* **2011**, *21*, 3178.
[15] X.-G. Han, H.-Z. He, Q. Kuang, X. Zhou, X.-H. Zhang, T. Xu, Z.-X. Xie, L.-S. Zheng, *J. Phys. Chem. C* **2009**, *113*, 584.
[16] X. Zhang, J. Qin, Y. Xue, P. Yu, B. Zhang, L. Wang, R. Liu, *Sci. Rep.* **2014**, *4*, 4596.
[17] K. Nomura, T. Kamiya, H. Ohta, M. Hirano, H. Hosono, *Appl. Phys. Lett.* **2008**, *93*, 192107.
[18] Y. S. Rim, W. H. Jeong, D. L. Kim, H. S. Lim, K. M. Kim, H. J. Kim, *J. Mater. Chem.* **2012**, *22*, 12491.
[19] H.-M. Xiong, D.-P Xie, X.-Y. Guan, Y.-J. Tan, Y.-Y. Xia, *J. Mater. Chem.* **2007**, *17*, 2490.
[20] J. Mei, M. S. Bradley, V. Bulović, *Phys. Rev. B* **2009**, *79*, 235205.
[21] W. J. E. Beek, M. M. Wienk, R. A. J. Janssen, *Adv. Mater.* **2004**, *16*, 1009.
[22] W. J. E. Beek, M. M. Wienk, R. A. J. Janssen, *Adv. Mater.* **2006**, *16*, 1112.
[23] J. S. Park, B. R. Lee, E. Jeong, H.-J. Lee, J. M. Lee, J.-S. Kim, J. Y. Kim, H. Y. Woo, S. O. Kim, M. H. Song, *Appl. Phys. Lett.* **2011**, *99*, 163305.
[24] H.-L. Yip, S. K. Hau, N. S. Baek, H. Ma, A. K.-Y. Jen, *Adv. Mater.* **2008**, *20*, 2376.
[25] S.-H. Oh, S.-I. Na, Y.-C. Nah, D. Vak, S.-S. Kim, D.-Y. Kim, *Org. Electron.* **2007**, *8*, 773.
[26] K.-Y. Pu, Z. Fang, B. Liu, *Adv. Funct. Mater.* **2008**, *18*, 1321.
[27] S. Lee, Y. Jeong, S. Jeong, J. Lee, M. Jeon, J. Moon, *Superlattice Microst.* **2008**, *44*, 761.
[28] J. Kim, D. Khim, R Kang, S.-H. Lee, K.-J. Baeg, M. Kang, Y.-Y. Noh, D.-Y. Kim, *ACS Appl. Mater. Interfaces* **2014**, *6*, 8108.
[29] S.-H. Oh, D. Vak, S.-I. Na, T.-W. Lee, D.-Y. Kim, *Adv. Mater.* **2008**, *20*, 1624.
[30] M. Elbing, A. Garcia, S. Urban, T.-Q. Nguyen, G. C. Bazan, *Macromolecules* **2008**, *41*, 9146.
[31] W. E. Morgan, J. R. Van Wazer, W. J. Stec, *J. Am. Chem. Soc.* **1973**, *95*, 751.
[32] R. D. Seals, R. Alexander, L. T. Taylor, J. G. Dillard, *Inorg. Chem.* **1973**, *12*, 2485.
[33] P. Atkins, T. Overton, J. Rourke, M. Weller, F. Armstrong, *Inorganic Chemistry*, 4th ed., Oxford University Press, Oxford, UK **2006**.
[34] D. K. Lavallee, J. Brace, N. Winograd, *Inorg. Chem.* **1979**, *18*, 1776.
[35] H. L. Mosbacker, S. El Hage, M. Gonzalez, S. A. Ringel, M. Hetzer, D. C. Look, G. Cantwell, J. Zhang, J. J. Song, L. J. Brillson, *J. Vac. Sci. Technol. B* **2007**, *25*, 1405.
[36] J. W. Stouwdam, R. A. J. Janssen, *J. Mater. Chem.* **2008**, *18*, 1889.
[37] B. R. Lee, E. D. Jung, Y. S. Nam, M. Jung, J. S. Park, S. Lee, H. Choi, S.-J. Ko, N. R. Shin, Y.-K. Kim, S. O. Kim, J. Y. Kim, H.-J. Shin, S. Cho, M. H. Song, *Adv. Mater.* **2014**, *26*, 494.
[38] B. R. Lee, E. D. Jung, J. S. Park, Y. S. Nam, S. H. Min, B.-S. Kim, K.-M. Lee, J.-R. Jeong, R. H. Friend, J.-S. Kim, S. O. Kim, M. H. Song, *Nat. Commun.* **2014**, *5*, 4840.